Title

Aberrant Ca2+ signaling by IP3Rs in adipocytes links inflammation to metabolic dysregulation in obesity.

Journal

Science Signaling, 14(713)

Authors

Cagampan, Erika

Min, Nina

Lee, Grace

et al.

Publication Date

2021-12-14

DOI

10.1126/scisignal.abf2059

Peer reviewed

HHS Public Access

Author manuscript

Sci Signal. Author manuscript; available in PMC 2023 April 26.

Published in final edited form as:

Sci Signal. 2021 December 14; 14(713): eabf2059. doi:10.1126/scisignal.abf2059.

Aberrant Ca^{2+} signaling by IP_3Rs in adipocytes links inflammation to metabolic dysregulation in obesity

Ekin Guney[1,*], **Ana Paula Arruda**[1,*,$], **Güneş Parlakgül**[1], **Erika Cagampan**[1], **Nina Min**[1], **Grace Yankun Lee**[1], **Lily Greene**[1], **Eva Tsaousidou**[1], **Karen Inouye**[1], **Myoung Sook Han**[2], **Roger J. Davis**[2], **Gökhan S. Hotamisligil**[1,3,$]

[1]Sabri Ülker Center for Metabolic Research and Department of Molecular Metabolism, Harvard T.H. Chan School of Public Health, Boston, MA 02115, USA.

[2]Program in Molecular Medicine, University of Massachusetts Medical School, Worcester, 01655, MA, USA.

[3]Broad Institute of MIT and Harvard, Cambridge, MA 02142, USA.

Abstract

Chronic metabolic inflammation is a key feature of obesity, insulin resistance, and diabetes. Here, we showed that altered regulation of the Ca^{2+} channel inositol trisphosphate receptor (IP3R) was an adipocyte-intrinsic event involved in the emergence and propagation of inflammatory signaling and the resulting insulin resistance. Inflammation induced by cytokine exposure in vitro or by obesity in vivo led to increases in the abundance and activity of IP3Rs and in the phosphorylation of the Ca^{2+}-dependent kinase CaMKII in adipocytes in a manner dependent on the kinase JNK. In mice, adipocyte-specific loss of IP3R1/2 protected against adipose tissue inflammation and insulin resistance, despite the mice exhibiting substantial diet-induced weight gain. Thus, this work suggests that increased IP3R activity is a key link between obesity, inflammation, and insulin resistance. These data also suggest that approaches to target IP3R-mediated Ca^{2+} homeostasis in adipocytes may offer new therapeutic opportunities against metabolic diseases, especially because GWAS studies also implicate this locus in human obesity.

Correspondence to: ghotamis@hsph.harvard.edu, aarruda@hsph.harvard.edu, 665 Huntington Ave. SPH2-117, Boston, MA, 02115, USA, Phone: 617 432-1952.

Author contributions:

E.G. and A.P.A. formulated the questions and performed the *in vitro* and *in vivo* experiments, analyzed the data and prepared the figures. G.P., E.C., N.M., E.T., K.I. performed and assisted with in vivo experiments. Y.L. and L.G. performed and assisted with in vitro experiments. M.S.H. and R.J.D. generated the adipocyte specific JNK1/2 deletion mouse model and performed the JNK1/2 studies. G.S.H. and A.P.A conceived and supervised the project, designed experiments, interpreted results, and wrote and revised the manuscript.

*These authors contributed equally to this work

$Co-Corresponding authors

Supplementary Materials

Fig. S1–S6.

Table S1.

Competing interests:

The authors declare that they have no competing interests.

Introduction:

White adipose tissue (WAT), which is composed of adipocytes, stromal cells, and immune cells, stores and disposes energy and has potent endocrine activity critical for the function and survival of the organism(1–4). Nutrient excess and obesity impose chronic pressure and stress on both the storage and endocrine functions of WAT. During chronic overnutrition, adipocytes become increasingly enlarged and dysfunctional and cannot buffer nutrients effectively, resulting in intracellular stress, recruitment of immune cells, and abnormal production and secretion of inflammatory molecules(1–5). Over time, this unfavorable situation ultimately results in tissue dysfunction and damage, systemic metabolic failure including insulin resistance, dyslipidemia, and metabolic disease.

Although the central role of WAT dysfunction in the development of metabolic diseases is recognized, important questions remain unanswered regarding the mechanisms associated with the emergence and propagation of inflammation in WAT. For example, the specific signals that determine the transition of adipocytes from a healthy to a dysfunctional phenotype during nutritional stress have not been identified, nor it is fully understood how metabolic inflammation is triggered and coupled to metabolic deterioration. At the cellular level, nutrient excess and the expansion of adipocytes lead to organelle stress, particularly in the endoplasmic reticulum (ER). Impaired ER function in the adipocytes is associated with unresolved ER unfolded protein response (UPR), in both mice and humans. However, how ER dysfunction is coupled to WAT inflammation and deterioration is not defined. In adipocytes, contrary to results in other metabolic cells such as hepatocytes, loss of function of the key UPR regulator XBP1(6) does not affect adipose tissue formation and function under homeostatic metabolic conditions and does not affect systemic metabolism in vivo. Thus, ER dysfunction in adipocytes and its impact in cell and systemic metabolism seem to present unique features that are not fully defined(7–11).

In *Drosophila melanogaster*, alterations in mechanisms that control ER Ca^{2+} homeostasis such as loss of function of the IP3R (inositol trisphosphate receptor), the ER channel responsible for Ca^{2+} release from ER to the cytosol, lead to obesity and altered lipid metabolism(12). In addition, loss of function in the fat body of the components of another key mechanism that control ER and cytosolic Ca^{2+} levels, store operated Ca^{2+} entry (SOCE), leads to marked lipid accumulation and obesity in the fly(13). Loss of function of SOCE in adipocytes in vitro also leads to alterations in lipid mobilization(14). Human genome-wide association studies (GWAS) have shown that an *ITPR* polymorphism is associated with increased body-mass index, fat mass(15) and waist-to-hip ratio(16) but not metabolic complications, and genotype-phenotype causality has yet to be established. These studies raise the possibility that regulation of intracellular Ca^{2+} homeostasis may be a key mechanism for adipose tissue metabolism. However, whether the regulation of ER Ca^{2+} handling affects organelle function in adipocytes or metabolic and inflammatory regulation in mammals has not been explored. The impact of intracellular Ca^{2+} homeostasis on adipocyte metabolism in general is a largely unexplored area.

In the present study, we identified a critical role for the IP3R Ca^{2+} channels as key drivers of adipocyte stress and adipose tissue inflammation. Through in vitro and in

vivo experiments, we demonstrated that IP3R abundance and activity in adipocytes were modulated by inflammatory cytokine exposure in vitro and by high fat diet (HFD)-induced inflammation in vivo in a mechanism dependent of the kinase JNK (c-Jun N-terminal kinase). Downregulation of IP3R isoforms in adipocytes decreased inflammatory signaling and metabolic dysfunction in vitro and in vivo, thus demonstrating that regulation of Ca^{2+} homeostasis in adipocytes is a key signal linking metabolic stress to inflammation and metabolic deterioration in obesity.

Results

Inflammation activates JNK-mediated phosphorylation of IP3R and CaMKII

To gain insight into a possible role of intracellular Ca^{2+} regulation in adipocyte dysfunction induced by inflammatory and metabolic stress, we first used an in vitro system in which we exposed differentiated 3T3-L1 adipocytes to a low dose of tumor necrosis factor α (TNFα), a pro-inflammatory cytokine elevated in obese mice and humans (1). Addition of TNFα to 3T3-L1 cells led to acute elevation of cytosolic Ca^{2+} (Fig. 1A). We then exposed 3T3-L1 cells to TNFα treatment (48 hours) and assessed adipocyte Ca^{2+} dynamics using the cytosolic Ca^{2+} indicator Fura2-AM (acetoxymethyl). Addition of the SERCA (sarco/endoplasmic reticulum Ca^{2+} -adenosine triphosphatase) inhibitor thapsigargin in the absence of extracellular Ca^{2+} led to lower cytosolic Ca^{2+} peak in cells pre-incubated with TNFα compared with untreated cells (Fig. 1B). The baseline Fura-2 signal was similar between treatments (fig. S1A). Addition of adenosine 5′-triphosphate (ATP), a purinergic receptor agonist that leads to IP3R activation through the generation of IP3, resulted in lower peak cytosolic Ca^{2+} in cells previously treated with TNFα (Fig. 1C). These results suggest that prolonged incubation with TNFα resulted in decreased ER Ca^{2+} content. Adipocytes treated with TNFα also showed increased CaMKII (calcium/calmodulin-dependent protein kinase II) phosphorylation (Fig.1D and fig.S1B), suggesting that TNFα treatment led to increased cytosolic Ca^{2+}. Next, we asked whether changes in adipocyte Ca^{2+} dynamics upon TNFα treatment were related to alterations of ER Ca^{2+} release. ER Ca^{2+} release is coordinated by the action of the IP3Rs and ryanodine receptors (RyRs). Upon detecting the predominant expression of *ITPRs* compared to *RYRs* mRNA in adipose tissue and adipocytes (fig.S1C and D), we focused on IP3Rs to explore the adipocyte Ca^{2+} homeostasis and its functional impact on metabolism. Treatment of adipocytes with TNFα led to a significant increase in IP3R1 phosphorylation at Ser^{1756}, an indicator of an open channel activity (Fig. 1E and F and fig. S1, E and F). Thus, TNFα induces elevation in cytosolic Ca^{2+} at least in part by modulating IP3R activity.

We then investigated the mechanism through which TNFα affects IP3R expression and phosphorylation in adipocytes. Given that JNK is a key inflammatory kinase downstream of inflammatory cytokines involved in metabolic homeostasis(17–19), we tested whether JNK mediates the effects of TNFα on IP3R abundance and phosphorylation in adipocytes. Suppression of JNK1/2 by small interfering RNA (siRNA) transfection led to a reduction in IP3R expression and prevented TNFα-induced IP3R1 phosphorylation (Fig. 2A, 2B and fig. S1G–I). In addition, the decreased ER Ca^{2+} content induced by TNFα treatment (Fig. 1B) was not detected in JNK1/2 deficient cells (Fig. 2C). Consistently, the induction of

CaMKII phosphorylation by TNFα triggered in control cells was significantly decreased in the absence of JNK1/2 in 3T3-L1 adipocytes (Fig. 2B and 2D). Together, these data reveal that activation of inflammatory signaling by TNFα in adipocytes leads to alterations in ER Ca^{2+} release and activation of Ca^{2+} dependent protein kinase CaMKII, a process downstream of the protein kinase JNK.

IP3R-mediated Ca^{2+} release is key for the inflammatory and metabolic actions of TNFα in adipocytes.

Next, we tested whether IP3R-induced Ca^{2+} release was involved in the inflammatory and metabolic actions of TNFα on differentiated 3T3-L1 adipocytes by knocking down IP3R1/2 and IP3R1/2/3 isoforms (fig. S2A–C). Downregulation of IP3R1/2/3 significantly inhibited ER-driven Ca^{2+} release stimulated by ATP (Fig. 3A). We did not observe differences in ATP-stimulated cytosolic Ca^{2+} elevation between cells in which IP3R1/2 or IP3R1/2/3 isoforms were downregulated, and thus, we downregulated only IP3R1/2 in subsequent experiments.

TNFα treatment of control adipocytes expressing scrambled siRNA led to a marked upregulation in the expression of mRNAs encoding pro-inflammatory cytokines and chemokines such as CCL2, CCL5, and CCL8, and inflammatory molecules such as iNOS, TNFα itself, and FasL receptor (Fig. 3B). In contrast, the expression of these mRNAs in response to TNFα was markedly diminished in adipocytes transfected with siRNAs targeting IP3R1/2 (Fig. 3B) or JNK1/2 (fig. S2D and S2E). To evaluate whether these effects resulted from changes in ER or cytosolic Ca^{2+} levels upon TNFα exposure, we treated 3T3-L1 cells with 1,2-bis(2-aminophenoxy)ethane-N,N,N′,N′- tetraacetic acid (BAPTA)-AM, a cytosolic Ca^{2+} chelator. BAPTA-AM co-treatment also significantly reduced TNFα-induced expression of mRNAs encoding chemokines and inflammatory molecules (Fig. 3C and fig. S2F). These data indicate a role for IP3Rs in the regulation of TNFα-driven inflammation in adipocytes.

In adipocytes, chronic low-grade TNFα treatment promotes insulin resistance through crosstalk between inflammatory and insulin signaling(5, 20, 21). We therefore asked whether decreasing IP3R activity by IP3R1/2 knockdown could prevent TNFα-induced insulin resistance in adipocytes. A low-dose TNFα treatment induced insulin resistance in control adipocytes, as evaluated by insulin-stimulated phosphorylation of insulin receptor (Fig. 3D and S2G). The inhibitory effect of TNFα on insulin signaling was attenuated in cells with downregulation of IP3R1/2 (Fig. 3D and fig. S2G) or JNK1/2 (fig. S2H). These results indicate a critical role for JNK-IP3R1 axis in both the inflammatory and metabolic activity of TNFα.

Obesity leads to increased IP3R content and activity in adipose tissue

We next explored the potential role of IP3Rs in adipose tissue dysfunction in vivo and in obesity. We first examined the impact of obesity on the expression levels of all three IP3R isoforms in epididymal white adipose tissue lysates (eWAT). The protein and mRNA expression levels of IP3R1–3 were markedly upregulated in mice fed an HFD (Fig. 4A and fig. S3A). Because the eWAT derived from obese animals contains large number of immune

cells, we asked whether the presence of IP3R channels reflected changes in expression in infiltrating cells or was intrinsic to adipocytes. To address this possibility, we fractionated the adipose tissue from lean [low fat diet (LFD)] and HFD fed mice to separate the stromal vascular fraction (SVF) from the buoyant adipocyte layer. Examination of adiponectin as a specific adipocyte marker confirmed the validity of the fractionation (fig. S3B). The increased expression of IP3R1/2 in HFD-fed mice was derived from the adipocytes, with no significant differences detected in the SVF fraction (Fig. 4B and 4C). We additionally evaluated the expression of IP3Rs in epididymal adipose tissue derived from a genetic model of obesity, leptin-deficient *ob/ob* mice. Similar to the profile observed in mice on HFD, eWAT derived from *ob/ob* mice also showed higher expression of IP3R1 and IP3R2 but not IP3R3 (Fig. 4D). To determine whether the increased quantity of IP3Rs in adipocytes affected cytosolic Ca^{2+} levels, we measured the phosphorylation status of CaMKII as a proxy for cytosolic Ca^{2+} (22, 23). We were not able to obtain consistent results when trying to measure cytosolic Ca^{2+} levels in adipose tissue in vivo with the available Ca^{2+} imaging reporters. In mice with either diet induced or genetically induced obesity, phosphorylation of CaMKII in eWAT was significantly elevated compared with their lean counterparts (Fig. 4A and 4D). These data support that obesity leads to altered Ca^{2+} homeostasis in adipocytes at least in part because of higher IP3R activity.

In cultured adipocytes, we found that enhanced IP3R expression and activity upon TNFα treatment required JNK1/2. We examined whether this was also the case in adipose tissue in vivo. Hence, we measured IP3R expression in eWAT derived from mice with adipocyte-specific loss of both JNK1/2. IP3R expression was significantly decreased in eWAT from JNK1/2 deficient mice maintained on LFD or HFD for 16 weeks (Fig. 5A, 5B and fig. S3C). IP3R1 and IP3R2 downregulation in mice with adipocyte-specific JNK1/2-deficiency was also observed at the mRNA levels (fig. S3D). In addition, the increased phosphorylation of CaMKII tended to be lower in the eWAT derived from JNK1/2 deficient mice (Fig.5A and fig. S3C). These results support a previously unrecognized role for JNK signaling in modulating IP3R abundance and activity in vitro and in vivo and also suggest that increased IP3Rs expression levels detected in adipose tissue during obesity may be a consequence of an inflammatory activation of JNK and may serve to integrate critical mechanistic nodes linking obesity and adipose tissue inflammation in vivo.

Loss of IP3R1/2 in adipose tissue protects from HFD-induced inflammation.

To investigate the impact of IP3Rs in adipocyte tissue metabolism in vivo, we generated mice with adipocyte-specific loss of function of IP3R1 and IP3R2 ($IP3R1/2^{AdpCre}$) by crossing mice with IP3R1 and IP3R2 (IP3R1/2) floxed alleles with mice expressing Cre recombinase under the control of adiponectin promoter (*Adp-Cre*) (fig. S4A). Expression of Cre recombinase in adipocytes from $IP3R1/2^{fl/fl}$ significantly decreased IP3R1/2 protein and mRNA levels as shown in multiple adipose depots, with no significant differences in the expression level of IP3R3 (fig. S4B, S4C and S4D). We then evaluated the impact of adipose tissue specific IP3R1/2 loss of function on body weight gain and energy expenditure in mice fed a LFD or HFD. On an LFD, body weight gain between genotypes was indistinguishable (fig. S4E). However, after 12 weeks on HFD, body weight gain between the groups diverged, and by 16 weeks, $IP3R1/2^{AdpCre}$ mice were 15 to 20% heavier than

control mice (Fig. 6A). Dual-energy x-ray absorptiometry (DEXA) analysis determined that the difference in body weight at 16 weeks of HFD was largely due to higher fat mass accumulation in *IP3R1/2*^{AdpCre} mice, and lean mass was similar between the genotypes (Fig. 6B). *IP3R1/2*^{AdpCre} mice also showed a tendency for decreased VO_2 and VCO_2 (fig. S4F and S4G), especially after the addition of the β3-agonist CL-316,243, although these differences were not statistically significant. No differences in body weight or food intake were observed at this time point (fig. S4H and S4I). Although intracellular Ca^{2+} regulation can influence lipolysis, we did not see significant differences in basal and isoproterenol -stimulated lipolysis in these mice (fig. S4J and S4K). These data indicate that IP3R1/2-deficiency leads to susceptibility to obesity and increased fat mass, similar to what has been observed in fruit flies(12) and in human GWAS studies(15, 16).

We next examined the effect of IP3R1/2 downregulation on adipose tissue inflammation and stress. In mice fed an LFD, there were no differences between genotypes in the inflammatory status of WAT (fig. S5A). However, obese *IP3R1/2*^{AdpCre} mice were markedly protected from immune infiltration of eWAT induced by 8 to 9 weeks of HFD feeding (Fig. 6C and fig. S5B), a time point when the body weights of both genotypes were similar. In addition, the expression of mRNAs encoding the inflammatory molecules CCL1, CCL5, CCL6, CXCL10, F4/80 and SAA3 was significantly reduced in eWAT from *IP3R1/2*^{AdpCre} compared to that from controls (Fig. 6D and fig. S5C). Liver steatosis was also significantly decreased in *IP3R1/2*^{AdpCre} mice compared with controls (fig. S5D). We then investigated the impact of IP3R1/2 loss on HFD-induced phosphorylation of CaMKII and of stress kinases downstream of inflammation such as JNK, p38, and extracellular signal–regulated kinase 1/2 (ERK1/2). IP3R1/2 loss of function in adipose tissue led to significantly decreased phosphorylation of CaMKII (Fig. 6E), suggesting that deletion of IP3R1/2 channels resulted in decreased adipocyte cytosolic Ca^{2+} levels in vivo. In addition, we detected that loss of IP3R1/2 also significantly inhibited the phosphorylation of p38 (Fig. 6E) and ERK (Fig. 6F) with no significant effect on the phosphorylation of JNK (Fig. 6F). This protection from inflammatory stress preceded the development of body weight differences between the groups (Fig. 6A). At the end of the 16 weeks on the HFD, expression of *CCL2* and *CCL5* remained significantly lower in the eWAT of *IP3R1/2*^{AdpCre} mice than in that of controls whereas the increase in the expression of mRNAs encoding other inflammatory molecules subsided (fig. S5E).

Loss of function of IP3R1/2 in adipose tissue protects against insulin resistance

Adipose tissue inflammation is closely associated with insulin resistance. Given the impact on IP3R1/2 deletion on decreasing inflammation and stress signaling in adipose tissue, we investigated the effect of IP3R1/2 deficiency in tissue and systemic glucose metabolism. In mice on an LFD, as with all other parameters measured, IP3R1/2 deletion in adipose tissue did not affect glucose tolerance and insulin sensitivity (fig. S6A and S6B). After 5 weeks on HFD, *IP3R1/2*^{AdpCre} mice exhibited a tendency of improved insulin sensitivity at the level of signaling proteins (fig. S6C), but this was not sufficient to alter systemic glucose or insulin tolerance (fig. S6D and S6E). At later times on the HFD (9 weeks), IP3R1/2^{AdpCre} mice exhibited improved insulin signaling in eWAT compared to IP3R1/2$^{fl/fl}$ mice, as demonstrated by a significant increase in the phosphorylation of insulin receptor (IR) and a

trend toward increased phosphorylation of AKT (Fig. 7A). Accordingly, *IP3R1/2*^{AdpCre} mice were more insulin sensitive as assessed by an insulin tolerance test (Fig. 7B). During an oral glucose tolerance test, the glucose excursion curves did not differ between *IP3R1/2*$^{fl/fl}$ and *IP3R1/2*^{AdpCre} (Fig. 7C). However, glucose-induced insulin secretion was significantly lower in *IP3R1/2*^{AdpCre} mice than in control mice (Fig.7D), indicating increased insulin sensitivity. Thus, adipose tissue-specific loss of function of IP3R1/2 increased diet-induced weight gain but protected against adipose tissue inflammation and insulin resistance and fatty liver development, thereby representing a metabolically healthy obese phenotype (Fig. 7E).

Discussion

The discovery of the immunometabolic nature of obesity and the central role of metabolic inflammation in adipose tissue dysfunction in obesity and diabetes have been followed up by a large amount of research connecting the immune response to metabolism and metabolic disease(1, 5, 20, 24, 25). However, the exact molecular events linking obesity-driven intracellular stress to the development and propagation of inflammation and subsequent metabolic pathologies have remained elusive and complex. Here, we showed that dysregulation of Ca^{2+} homeostasis at the level of the ER Ca^{2+} channel IP3Rs is a key, previously unrecognized link integrating these mechanistic processes into a cohesive model of pathogenesis. Specifically, we showed that inflammation, modeled in cells in vitro or during the course of obesity in vivo, led to enhanced expression and activation of the ER Ca^{2+} channel IP3R in adipocytes, leading to lower ER Ca^{2+} content and activation of CaMKII, which has important implications in inflammatory signaling and the development of insulin resistance.

The cycle of increased IP3R1 expression and activity promoted by inflammatory stress and chronic overnutrition is prevented in the absence of JNK1/2, suggesting that JNK is a key upstream factor that regulates IP3R induced Ca^{2+} release and CaMKII phosphorylation in adipocytes. Although JNK has been suggested to regulate IP3R1 expression at the transcriptional level in a neuronal cell line(26), it is possible that JNK also regulates IP3R1 activity through other mechanisms such as post-translational modification. Mice deficient in JNK in adipose tissue are protected against metabolic disease, even when challenged by an HFD, although their body weight does not differ from control mice (27). Our data suggest that this protection may be at least partially mediated by decreased IP3R-driven Ca^{2+} release in JNK1/2 deficient adipocytes.

Inhibition of the rise in cytosolic Ca^{2+}, by either downregulation of IP3R expression or treatment with the Ca^{2+} chelator BAPTA, diminished the inflammatory cascades triggered by TNFα in cultured adipocytes and adipose tissue inflammation and immune cell infiltration promoted by HFD in vivo. An important impact of the attenuation of inflammatory signaling by downregulation of IP3R1/2 treatment was rescue of the insulin resistance caused by inflammatory stress in vitro and nutritional stress in vivo, implicating regulation of insulin action by IP3R activity. Inhibition of TRPV4, a non-selective Ca^{2+} channel, has also been reported to reduce adipose tissue inflammation(28) and cytosolic Ca^{2+} has been linked to insulin signaling through a CaMKII-P38-ATF6 axis in the

liver(29). In our model, CaMKII and p38 phosphorylation were both decreased by IP3R1/2 downregulation in adipose tissue, suggesting that the crosstalk between cytosolic Ca^{2+} and insulin signaling in adipose tissue may be mediated by these kinases. It is possible that other Ca^{2+}-regulated mechanisms contribute to this phenomenon, such as alterations in mitochondrial Ca^{2+} and oxidative stress. Additional work will be necessary to understand how IP3R modulation affects mitochondrial Ca^{2+} levels and function in adipose tissue.

In summary, our work demonstrates that proper regulation of the Ca^{2+} channel activity of IP3Rs is a central process for the maintenance of adipocyte metabolic health, and alterations of this fine balance are a signal that leads to adipocyte dysfunction in the context of obesity. Together with the role of dysregulated IP3R content and activity in the liver in altered hepatic glucose production(30–33), the observations shown here suggest that imbalance in intracellular Ca^{2+} at the IP3R level is a major pillar of metabolic homeostasis and alterations in its function collectively predispose to overall metabolic defects(29–33). Moreover, this mechanism seems to be conserved across different organisms, because loss of function of IP3R(12) and SOCE(13) in the fat body in *Drosophila* leads to increased adiposity. IP3R1/2 deficiency in adipose tissue leads to development of greater adiposity uncoupled from metabolic complications, possibly representing a model of metabolically healthy obesity, which would be consistent with the phenotypes observed in human GWAS studies. Therefore, our work supports the idea that preventing aberrant IP3R activity could be a powerful strategy to rescue systemic glucose metabolism and inflammatory stress in obesity. Pharmacological attempts in this direction are being developed such as the use of SERCA agonists(34) or azoramide(35), although it remains to be elucidated whether targeting this mechanism can safely improve metabolism in humans.

Materials and Methods:

General animal care and study design

All *in vivo* studies were approved by the Harvard Medical Area Standing Committee on Animals. Unless stated otherwise, mice were maintained from 4–20 weeks of age on a 12-hour-light /12-hour-dark cycle in the Harvard T.H. Chan School of Public Health pathogen-free barrier facility with free access to water and to a standard laboratory chow diet (PicoLab Mouse Diet 20 #5058, LabDiet). The sample size and number of replicates for this study were chosen based on previous experiments performed in our laboratory and others(31, 36).

Animal models

WT, heterozygous and leptin-deficient Lep^{ob} (*ob*/*ob*) mice (Stock no. 000632) were purchased from Jackson Laboratories at 6–7 weeks of age and used for experimentation between 8–10 weeks of age. For diet-induced obesity, male C57BL/6J mice were purchased from Jackson Laboratories and placed on HFD (D12492: 60% kcal% fat; Research Diets) for up to 26 weeks. Control mice of the same age were fed with a low-fat diet (PicoLab Mouse Diet 20 #5053, LabDiet).

Mice carrying floxed alleles for IP3R1 and IP3R2 (Fig. 5A) were kindly provided by Dr. Andrew Marks from Columbia University Medical Center(37, 38). To generate adipocyte-specific IP3R1/2 deficient mice, *IP3R1*$^{fl/fl}$ and *IP3R2*$^{fl/fl}$ mice were bred to C57BL/6J mice expressing CRE recombinase under the control of the adiponectin promoter (Adp-Cre, Jax stock #028020). Adp-Cre-mediated recombination of floxed IP3R1/2 alleles was detected in genomic DNA by PCR performed with the following protocol: 3 minutes at 95^0C, 35 times repeats of (30 seconds at 95^0C, 30 seconds at 60^0C, 45 seconds at 72^0C), 3 minutes at 72^0C and hold at 4^0C. Products of PCR were as follows; *IP3R1*-WT: 320bp; *IP3R1*-floxed: 406bp; *IP3R2*-WT: 248 bp, IP3R2-floxed: 394 bp. The genetic background of the mice was determined to be 93–98% C57BL/6. Age-matched littermates were used for the study. Mice were placed on HFD (D12492: 60% kcal% fat; Research Diets) from 6 up to 20 weeks. The control chow group were switched from chow-diet (PicoLab Mouse Diet 20 #5058, LabDiet) to low-fat chow diet (PicoLab Mouse Diet 20 #5053, LabDiet) at 6 weeks of age and remained on this diet for the same period as the mice on the HFD.

Mice carrying floxed alleles for JNK1 and JNK2 were generated in Dr. Roger Davis's laboratory at the Program in Molecular Medicine, UMASS Medical School. *JNK1/2* wild type mice crossed with mice carrying Cre recombinase under the control of Adiponectin promoter was used as controls. *JNK1/2* flox/flox mice crossed with mice carrying Cre recombinase under control of *Adiponectin* promoter was used to delete JNK1/2 specifically in adipocytes. Age-matched mice were used for the study. Mice were placed on the HFD for up to 16 weeks. The LFD was Purina Cat# IsoPro3000 and the HFD was Bioserv # S3282.

Indirect Calorimetry

Mouse oxygen consumption and carbon dioxide emission were measured using a Columbus Instruments Oxymax-Comprehensive Lab Animal Monitoring System (CLAMS) system, according to guidelines for measuring energy metabolism in mice(39). We measured brown adipose tissue-mediated respiration by intrapertoneal injection of the β3 adrenergic receptor-specific agonist CL316,243 (CL, Tocris, 0.5 mg/kg in 0.9 % w/v in NaCl).

Glucose and insulin tolerance tests

For the glucose tolerance tests, mice were administered glucose by oral gavage after overnight fasting (lean: 1.5 g kg^{-1}, obese: 0.5–1.0 g kg^{-1}), and blood glucose levels were measured throughout 120 minutes as indicated in the figures. For insulin tolerance tests, insulin was injected intraperitoneally (0.75–1U/ kg^{-1}) after 6h food withdrawal and blood glucose levels were measured throughout 120 minutes as indicated in the figures.

Lipolysis

Mice were injected intraperitoneally with isoproterenol (10mg/kg in PBS, Tocris) after 6h food withdrawal. Blood was collected by tail vein during a 60-minute period as indicated in figs. S4J and S4K. Free fatty acids and glycerol were determined in the plasma.

SVF and adipocyte isolation

Epididymal adipose tissue was collected in PBS, washed twice with fresh PBS and transferred into 10 cm petri-dishes on ice containing enzymatic digestion buffer (Krebs-

Ringer solution, 2% BSA, Collagenase type-I (1.25mg powder/1ml); 4–5 ml/mouse for lean mice and 7–8 ml/HFD mouse). Immediately after, tissue was minced using surgical scissors for 5–10 minutes until each piece was smaller than 1 mm. The mixture of minced adipose tissue and enzymatic digestion buffer was transferred into 50 ml conical tube and placed on ice. Once this procedure was completed for each mouse, the mixtures were transferred into a shaker and incubated for 45–60 minutes at 37^0C at 100 rpm until all adipose tissue fragments were digested completely. Digested mixtures were filtered using 200um strainers (pluriStrainer 200 μm (Cell Strainer); Catalog ID: 43-50200-03). For adipocyte fraction preparation, the supernatant adipocyte fraction was collected and transferred into 15 ml conical tubes which was then brought up to 10 mL volume by the addition of Krebs-ringer-2%BSA-mixture followed by centrifugation at 300 rpm for 10 min at 4^0C. Following centrifugation, supernatant adipose tissue fraction was transferred into 1.5 ml tubes, which were then centrifuged at 300 rpm for 10 min. Supernatant buffer was then removed, lysis buffer was added, and the protein lysate was prepared as described for whole tissue. For stromal-vascular fraction (SVF) preparation, the buffer between the supernatant and the pellet was removed and the remaining pellet was mixed with PBS and centrifuged at 3000 rpm for 5 minutes at 4^0C. Following centrifugation, the supernatant buffer was removed, lysis buffer was added to the remaining pellet and protein lysate was prepared as described for whole tissue.

Histological analysis

Adipose and liver tissues were fixed in 10% zinc-formalin for 24 h at room temperature and transferred to 70% ethanol for further storage. Tissues were processed, sectioned and stained with hematoxylin and eosin at the Dana Farber Rodent Histopathology facility at Harvard Medical School. Hepatic steatosis scoring was based on a previously described method (40). Adipose tissue inflammation was evaluated subjectively taking into consideration number and size of inflammatory infiltrates. The inflammatory foci were given a score between 0–3, where 0 represented no inflammation, 1 was moderate, and 3 was pronounced inflammation.

Adipocyte differentiation

3T3-L1 cells (American Type Culture Collection) were seeded into culture dishes at about 70% confluence in Dulbecco's modified Eagle's medium (DMEM) with 4.5 mM glucose (GIBCO) supplemented with 10% bovine calf serum and 1% penicillin/streptomycin. Once the cells reached 100% confluence (2–3 days after seeding), the medium was changed to DMEM with 10% fetal bovine serum (FBS) with 1% penicillin/streptomycin. After 2 days (day 0), adipocyte differentiation was induced by the addition of 500 μM 3-isobutyl-1-methylxanthine (IBMX), 5 μg/ml insulin, 10 μM dexamethasone, and 10 μM rosiglitazone. On day 2, the medium was switched to DMEM with 10% FBS and 1% penicillin/streptomycin, 5 μg/ml insulin and 10 μM rosiglitazone. On day 4, the medium was switched to DMEM with 10% FBS and 1% penicillin/streptomycin (maintenance medium), which was replaced every other day until day 10, when the adipocytes were fully differentiated. Experiments were performed on day 10. Recombinant murine-TNFα (cat number: 315–01A, PeproTech) was dissolved in nuclease-free sterile water and diluted according to the user's manual. The main stock was prepared at concentration of 100 μg/mL and aliquoted to prevent freeze-thaw cycles. TNFα was diluted to 4 ng/ml in the

maintenance medium and added to cells for the period of time described in the experiments at 37°C. After TNFα treatment, the medium was removed, wells were washed with PBS and the tissue culture plates were frozen in liquid nitrogen. For experiments involving BAPTA-AM (cat number: A1076, Sigma-Aldrich), main stocks were prepared at 10 mM in DMSO according to the user's manual and diluted to 1 μM or 10 μM in maintenance medium. The amount of DMSO in the BAPTA-AM solution was added to TNFα-only and control medium treatment mixtures. For TNFα treatment experiments, treatment mixtures were prepared as TNFα-only (with DMSO), TNFα with BAPTA-AM, BAPTA-AM-only, and control medium (with DMSO). Treatment mixtures were added simultaneously, and culture plates were incubated at 37^0C.

Transfections

After 10 days of differentiation, adipocytes were transfected with scrambled or IP3R1/2/3 siRNA (separately or in combination) or JNK1/2 siRNA. For the transfection, cells were trypsinized (0.25% trypsin), transferred into 15 ml conical tubes and centrifuged for 10 minutes at 300 rpm at 4^0C. The supernatant was removed, and the pellets were diluted in transfection media (DMEM, 10%FBS, no penicillin/streptomycin). The adipocytes were counted and seeded in 6 or 12-well plates (5×10^5 cells/well for 6-well plates and 2.5×10^5 cells/well for 12-well plates; at approximately 70% confluence). Lipofectamine-RNAiMax (Catalog number: 13778030) and Opti-MEM medium were from Thermo Fisher Scientific; Mouse-siRNAs for On-target SMARTpool scrambled-control, ITPR1 (catalog ID: L-040933-00-0005), ITPR2 (L-041018-00-0005), ITPR3 (L-065715-01-0005), Mapk8 (L-040128-00-0005) and Mapk9 (L-040134-00) were from Dharmacon. Transfection mixtures were prepared following the lipofectamine-RNAiMAX-transfection protocol. The transfection mixture (300μl/well for 6-well plate) was added to the wells containing adipocytes, bringing the total volume of the wells up to 2.2 ml. The culture plates were incubated in 37^0C incubators for 16 hours. After 16 hours, medium was replaced with maintenance medium and plates were incubated until 36 hours after the transfection before the experiments.

Insulin signaling

3T3-L1 cells transfected with scrambled or IP3R1/2 siRNA were treated with 4ng/mL of TNFα for 4 days. Media was changed every 24-hours. After 96 hours (4 replacements), cells were washed with warm (37^0C) PBS three times and serum-free medium was added into the wells (6-well plates) for 6 hours at 37^0C. Insulin solutions were prepared in serum-free medium (1, 10 and 100 nM). After 6 hours, the cells were treated with serum-free medium with or without 3nM insulin solution for 3 minutes. After insulin treatment wells were washed twice with cold PBS and frozen in liquid nitrogen.

Cytosolic Ca^{2+} imaging using Fura-2 AM

Cells were loaded with 4 μM Fura-2AM and 1 μM Pluronic F-127 in HBSS for ~25 to 60 min at room temperature. Before imaging, the cells were washed and kept in a medium containing 10 mM HEPES, 150 mM NaCl, 4 mM KCl, 2 mM $CaCl_2$, 1 mM $MgCl_2$, 10 mM D-glucose, pH 7.4 for 5 minutes. Ca^{2+}-free medium was prepared similarly to the buffer described above, in the absence of $CaCl_2$ and in the presence of 2 mM EGTA and

3 mM $MgCl_2$. Ratiometric Fura-2AM imaging was performed with a **Nikon Ti-S Inverted Microscope** alternatively illuminated with 340 and 380 nm light for 250 ms (Lambda DG-4; Sutter Instrument Co.), using a 20X objective, Nikon CFI Super Fluor. Emission light > 510 nm was captured using a Zyla 4.2 scientific complementary AQ9 metal-oxide semiconductor camera (Andor). Both channels were collected every 5 seconds with NIS-Elements software. Images were background corrected and analyzed in image J. Average of traces of stimulant responsive cells are shown in the figures.

Total protein extraction and Western blotting

Adipose tissues were homogenized in cold lysis buffer containing 50 mM Tris-HCl (pH 7.4), 2 mM EGTA, 5 mM EDTA, 30 mM NaF, 10 mM Na_3VO_4, 10 mM $Na_4P_2O_7$, 40 mM glycerophosphate, 1% NP-40, and 1% protease inhibitor cocktail or radioimmunoprecipitation assay buffer (Cell Signaling Technology, 9806) supplemented by 1% protease inhibitor cocktail. Adipose tissue was homogenized using a polytron in cold lysis buffer. Homogenates were placed on ice for 45 minutes and intermittently vortexed. The homogenates were centrifuged for 15 minutes at 9000 rpm to pellet cell debris. The supernatant with the protein lysate was collected and the centrifugation was repeated once more. Protein concentrations were determined by BCA. Samples were diluted in 5x Laemmli buffer and boiled for 5 minutes 95^0C. The protein lysates were subjected to SDS-polyacrylamide gel electrophoresis, as previously described(31, 35). Membranes were incubated with anti- JNK (Cell signaling #9252), anti-pAKT-Rabbit Antibody(Ser473) (Cell Signaling #9271), anti-AKT-Rabbit Antibody (Cell Signaling #9272),anti-IR (Santa Cruz 711), p-Insulin Receptor Antibody(p-Thy1162/1163) (Calbiochem 407707 or Sigma I1783), phospho-CaM KinaseII (Cell Signaling #12716), CamKII (pan) (Cell Signaling #3362), pIP3R1 (Cell signaling #3760), IP3R1 (Bethyl Laboratories – A392–158A), IP3R2 (received as a kind gift from Dr Wojcikiewicz, Upstate Medical University), purified mouse anti-IP3R3 (BD Transduction Laboratories), BiP (Cell Signaling #3183), Calnexin (Santa Cruz, sc-6465), Adiponectin-Acrp30 (G-17 clone,sc-26496), β-tubulin (Abcam, ab 21058).

Gene expression analysis by qPCR

Tissues were homogenized in Trizol (Invitrogen) using TissueLyser (Qiagen). To obtain RNA, Trizol homogenates were mixed with chloroform, vortexed thoroughly and centrifuged at 12000g for 20 min at 4°C. The top layer was transferred to another tube and mixed with isopropanol and centrifuged again at 12000g for 20 min at 4°C. The RNA in the precipitate was washed twice with 70% ethanol and diluted in RNAse free water. Complementary DNA was synthesized using iScript RT Supermix kit (Biorad). Quantitative real-time PCR reactions were performed in duplicates or triplicates on a ViiA7 system (Applied Biosystems) using SYBR green and custom primer sets or based on Harvard primer bank. Gene of interest cycle thresholds (Cts) were normalized to TBP housekeeping levels by the ΔΔCt. The primers used in all the qPCR analyses are shown in table S1.
In fig S3D, mRNA expression was examined by quantitative RT-PCR analysis using a Quantstudio machine (ThermoFisher Scientific). TaqMan assays were used to quantify *Itpr1* (Mm00439907_m1), *Itpr2* (Mm00444937_m1), and *Itpr3* (Mm01306070_m1) mRNA (ThermoFisher Scientific).

Statistical Analysis

Statistical significance was assessed using GraphPad Prism Version 7. One-way ANOVA (Dunnett post-Hoc test) was used for Fig 1E and 3C. Two-way ANOVA (Sidak post-Hoc test) was used for Fig 6B, 7B and 7D. Mann Whitney test (two-sided) was used for Fig. 1B, 1C and 3A. Unpaired t-tests (two-sided) was used for all other figures. All data is mean ± SEM.

Supplementary Material

Refer to Web version on PubMed Central for supplementary material.

Acknowledgments:

We are grateful to A. Marks from Columbia University, NY for providing us with the IP3R1 and IP3R2 floxed mice. We thank R. Wojcikiewicz from Upstate Medical University for sending us the IP3R2 antibody generated in his laboratory. We thank K. Claiborn for critical reading and editing of the manuscript. We thank all members of the Sabri Ülker Center and Hotamisligil Lab community for their continued support and encouragement.

Funding:

This work is supported by the Sabri Ülker Center for Metabolic Research. G.P. is supported by an NIH training grant (5T32DK007529-32). E.T. is supported by AHA postdoctoral fellowship (18POST33990109). R.J.D. is supported by NIH R01 DK112698. M.S.H. is supported by AHA Career Development Award (19CDA34660270).

Data and materials availability:

All data needed to evaluate the conclusions in the paper are present in the paper or the Supplementary Materials. Uncropped versions of the Western blots used in the figures can be accessed at https://doi.org/10.6084/m9.figshare.17109140. IP3R1 and IP3R2 floxed mice were obtained from A. Marks from Columbia University Medical Center under a material transfer agreement (MTA) between Columbia University and Harvard University. The JNK1/JNK2 floxed mice are from R. J. Davis from University of Massachusetts Medical School and requires an MTA.

References and Notes:

1. Hotamisligil GS, Inflammation, metaflammation and immunometabolic disorders. Nature. 542, 177–185 (2017). [PubMed: 28179656]
2. Scherer PE, The many secret lives of adipocytes: implications for diabetes. Diabetologia. 62 (2019), pp. 223–232. [PubMed: 30465066]
3. Kusminski CM, Bickel PE, Scherer PE, Targeting adipose tissue in the treatment of obesity-associated diabetes. Nat. Rev. Drug Discov 15 (2016), pp. 639–660. [PubMed: 27256476]
4. Rosen ED, Spiegelman BM, What we talk about when we talk about fat. Cell. 156 (2014), pp. 20–44. [PubMed: 24439368]
5. Lercher A, Baazim H, Bergthaler A, Systemic Immunometabolism: Challenges and Opportunities. Immunity. 53 (2020), pp. 496–509. [PubMed: 32937151]
6. Gregor MF, Misch ES, Yang L, Hummasti S, Inouye KE, Lee AH, Bierie B, Hotamisligil GS, The Role of Adipocyte XBP1 in Metabolic Regulation during Lactation. Cell Rep. 3, 1430–1439 (2013). [PubMed: 23623498]
7. Hotamisligil GS, Endoplasmic Reticulum Stress and the Inflammatory Basis of Metabolic Disease. Cell. 140, 900–917 (2010). [PubMed: 20303879]

8. Khan S, Wang CH, ER stress in adipocytes and insulin resistance: Mechanisms and significance (Review). Mol. Med. Rep 10, 2234–2240 (2014). [PubMed: 25189738]
9. Özcan U, Cao Q, Yilmaz E, Lee AH, Iwakoshi NN, Özdelen E, Tuncman G, Görgün C, Glimcher LH, Hotamisligil GS, Endoplasmic reticulum stress links obesity, insulin action, and type 2 diabetes. Science (80-.). 306, 457–461 (2004).
10. Gregor MF, Yang L, Fabbrini E, Mohammed BS, Eagon JC, Hotamisligil GS, Klein S, Endoplasmic reticulum stress is reduced in tissues of obese subjects after weight loss. Diabetes. 58, 693–700 (2009). [PubMed: 19066313]
11. Gardner BM, Pincus D, Gotthardt K, Gallagher CM, Walter P, Endoplasmic reticulum stress sensing in the unfolded protein response. Cold Spring Harb. Perspect. Biol 5 (2013), doi:10.1101/cshperspect.a013169.
12. Subramanian M, Metya SK, Sadaf S, Kumar S, Schwudke D, Hasan G, Altered lipid homeostasis in Drosophila InsP3 receptor mutants leads to obesity and hyperphagia. DMM Dis. Model. Mech 6, 734–744 (2013). [PubMed: 23471909]
13. Baumbach J, Hummel P, Bickmeyer I, Kowalczyk KM, Frank M, Knorr K, Hildebrandt A, Riedel D, Jäckle H, Kühnlein RP, A drosophila in vivo screen identifies store-operated calcium entry as a key regulator of adiposity. Cell Metab. 19, 331–343 (2014). [PubMed: 24506874]
14. Maus M, Cuk M, Patel B, Lian J, Ouimet M, Kaufmann U, Yang J, Horvath R, Hornig-Do HT, Chrzanowska-Lightowlers ZM, Moore KJ, Cuervo AM, Feske S, Store-Operated Ca2+ Entry Controls Induction of Lipolysis and the Transcriptional Reprogramming to Lipid Metabolism. Cell Metab. 25, 698–712 (2017). [PubMed: 28132808]
15. Mao L, Fang Y, Campbell M, Southerland WM, Population differentiation in allele frequencies of obesity-associated SNPs. BMC Genomics. 18 (2017), doi:10.1186/s12864-017-4262-9.
16. Shungin D, et al. , New genetic loci link adipose and insulin biology to body fat distribution. Nature. 518, 187–196 (2015). [PubMed: 25673412]
17. Hirosumi J, Tuncman G, Chang L, Görgün CZ, Uysal KT, Maeda K, Karin M, Hotamisligil GS, A central, role for JNK in obesity and insulin resistance. Nature. 420, 333–336 (2002). [PubMed: 12447443]
18. Hotamisligil GS, Davis RJ, Cell signaling and stress responses. Cold Spring Harb. Perspect. Biol 8 (2016), doi:10.1101/cshperspect.a006072.
19. Weston CR, Davis RJ, The JNK signal transduction pathway. Curr. Opin. Cell Biol 19 (2007), pp. 142–149. [PubMed: 17303404]
20. Hotamisligil GS, Shargill NS, Spiegelman BM, Adipose expression of tumor necrosis factor-α: Direct role in obesity-linked insulin resistance. Science (80-.). 259, 87–91 (1993).
21. Liang H, Yin B, Zhang H, Zhang S, Zeng Q, Wang J, Jiang X, Yuan L, Wang CY, Li Z, Blockade of tumor necrosis factor (TNF) receptor type 1-mediated TNF-α signaling protected Wistar rats from diet-induced obesity and insulin resistance. Endocrinology. 149, 2943–2951 (2008). [PubMed: 18339717]
22. Ozcan L, Wong CCL, Li G, Xu T, Pajvani U, Park SKR, Wronska A, Chen BX, Marks AR, Fukamizu A, Backs J, Singer HA, Yates JR, Accili D, Tabas I, Calcium signaling through CaMKII regulates hepatic glucose production in fasting and obesity. Cell Metab. 15, 739–751 (2012). [PubMed: 22503562]
23. Perry RJ, Zhang D, Guerra MT, Brill AL, Goedeke L, Nasiri AR, Rabin-Court A, Wang Y, Peng L, Dufour S, Zhang Y, Zhang XM, Butrico GM, Toussaint K, Nozaki Y, Cline GW, Petersen KF, Nathanson MH, Ehrlich BE, Shulman GI, Glucagon stimulates gluconeogenesis by INSP3R1-mediated hepatic lipolysis. Nature. 579, 279–283 (2020). [PubMed: 32132708]
24. Arkan MC, Hevener AL, Greten FR, Maeda S, Li ZW, Long JM, Wynshaw-Boris A, Poli G, Olefsky J, Karin M, IKK-β links inflammation to obesity-induced insulin resistance. Nat. Med 11, 191–198 (2005). [PubMed: 15685170]
25. Saltiel AR, Olefsky JM, Inflammatory mechanisms linking obesity and metabolic disease. J. Clin. Invest 127, 1–4 (2017). [PubMed: 28045402]
26. Park KM, Yule DI, Bowers WJ, Tumor necrosis factor-α-mediated regulation of the inositol 1,4,5-trisphosphate receptor promoter. J. Biol. Chem 284, 27557–27566 (2009). [PubMed: 19666470]

27. Han MS, Perry RJ, Camporez JP, Scherer PE, Shulman GI, Gao G, Davis RJ, A feed-forward regulatory loop in adipose tissue promotes signaling by the hepatokine FGF21. Genes Dev. 35, 133–146 (2021). [PubMed: 33334822]
28. Ye L, Kleiner S, Wu J, Sah R, Gupta RK, Banks AS, Cohen P, Khandekar MJ, Boström P, Mepani RJ, Laznik D, Kamenecka TM, Song X, Liedtke W, Mootha VK, Puigserver P, Griffin PR, Clapham DE, Spiegelman BM, TRPV4 is a regulator of adipose oxidative metabolism, inflammation, and energy homeostasis. Cell. 151, 96–110 (2012). [PubMed: 23021218]
29. Ozcan L, Cristina De Souza J, Harari AA, Backs J, Olson EN, Tabas I, Activation of calcium/calmodulin-dependent protein kinase II in obesity mediates suppression of hepatic insulin signaling. Cell Metab. 18, 803–815 (2013). [PubMed: 24268736]
30. Arruda AP, Hotamisligil GS, Calcium homeostasis and organelle function in the pathogenesis of obesity and diabetes. Cell Metab. 22, 381–397 (2015). [PubMed: 26190652]
31. Arruda AP, Pers BM, Parlakgül G, Güney E, Inouye K, Hotamisligil GS, Chronic enrichment of hepatic endoplasmic reticulum-mitochondria contact leads to mitochondrial dysfunction in obesity. Nat. Med 20, 1427–1435 (2014). [PubMed: 25419710]
32. Arruda AP, Pers BM, Parlakgul G, Güney E, Goh T, Cagampan E, Lee GY, Goncalves RL, Hotamisligil GS, Defective STIM-mediated store operated Ca2+ entry in hepatocytes leads to metabolic dysfunction in obesity. Elife. 6 (2017), doi:10.7554/eLife.29968.
33. Wang Y, Li G, Goode J, Paz JC, Ouyang K, Screaton R, Fischer WH, Chen J, Tabas I, Montminy M, Inositol-1,4,5-trisphosphate receptor regulates hepatic gluconeogenesis in fasting and diabetes. Nature. 485, 128–132 (2012). [PubMed: 22495310]
34. Kang S, Dahl R, Hsieh W, Shin A, Zsebo KM, Buettner C, Hajjar RJ, Lebeche D, Small molecular allosteric activator of the sarco/endoplasmic reticulum Ca2+-ATPase (SERCA) attenuates diabetes and metabolic disorders. J. Biol. Chem 291, 5185–5198 (2016). [PubMed: 26702054]
35. Fu S, Yalcin A, Lee GY, Li P, Fan J, Arruda AP, Pers BM, Yilmaz M, Eguchi K, Hotamisligil GS, Phenotypic assays identify azoramide as a small-molecule modulator of the unfolded protein response with antidiabetic activity. Sci. Transl. Med 7 (2015), doi:10.1126/scitranslmed.aaa9134.
36. Fu S, Yang L, Li P, Hofmann O, Dicker L, Hide W, Lin X, Watkins SM, Ivanov AR, Hotamisligil GS, Aberrant lipid metabolism disrupts calcium homeostasis causing liver endoplasmic reticulum stress in obesity. Nature. 473, 528–531 (2011). [PubMed: 21532591]
37. Santulli G, Xie W, Reiken SR, Marks AR, Mitochondrial calcium overload is a key determinant in heart failure. Proc. Natl. Acad. Sci. U. S. A 112, 11389–11394 (2015). [PubMed: 26217001]
38. Yuan Q, Yang J, Santulli G, Reiken SR, Wronska A, Kim MM, Osborne BW, Lacampagne A, Yin Y, Marks AR, Maintenance of normal blood pressure is dependent on IP3R1-mediated regulation of eNOS. Proc. Natl. Acad. Sci. U. S. A 113, 8532–8537 (2016). [PubMed: 27402766]
39. Bartelt A, Widenmaier SB, Schlein C, Johann K, Goncalves RLS, Eguchi K, Fischer AW, Parlakgül G, Snyder NA, Nguyen TB, Bruns OT, Franke D, Bawendi MG, Lynes MD, Leiria LO, Tseng YH, Inouye KE, Arruda AP, Hotamisligil GS, Brown adipose tissue thermogenic adaptation requires Nrf1-mediated proteasomal activity. Nat. Med 24, 292–303 (2018). [PubMed: 29400713]
40. Takahashi Y, Fukusato T, Histopathology of nonalcoholic fatty liver disease/nonalcoholic steatohepatitis. World J. Gastroenterol 20, 15539–15548 (2014). [PubMed: 25400438]

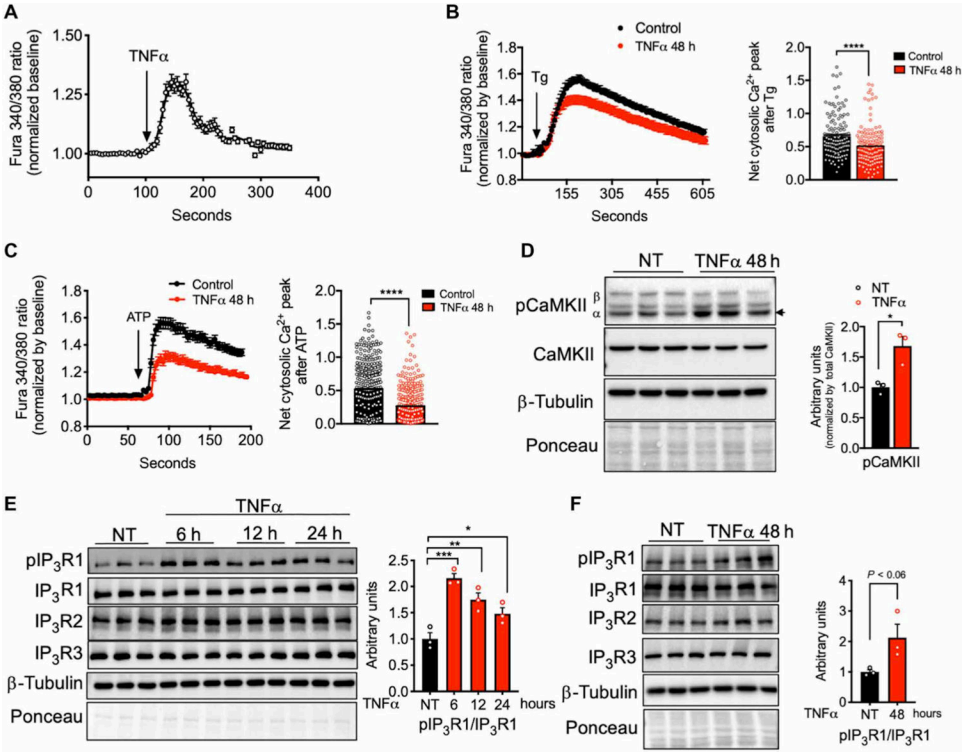

Fig. 1. Inflammatory stress leads to increased IP3R expression and activity in adipocytes.

(**A**) Representative Fura-2 AM–based cytosolic Ca^{2+} measurements in differentiated 3T3-L1 adipocytes treated with TNFα (50 ng/ml). n=30 cells. (**B**) Left: Representative Fura-2 AM–based cytosolic Ca2+ measurements in differentiated 3T3-L1 pretreated with TNFα (4 ng/ml) for 48 hours. ER Ca^{2+} depletion was stimulated with 1 μM thapsigargin (SERCA inhibitor) in medium with no extracellular Ca^{2+}. n=36 cells for controls and 28 cells for TNFα. Right: Quantification of Ca^{2+} peak normalized to baseline. n=140 control and 142 TNFα, averaged from four different biological replicates per condition. ****P<0.0001. (**C**) Left: Representative Fura-2 AM–based cytosolic Ca^{2+} measurements in differentiated 3T3-L1 pretreated with TNFα (4 ng/ml) for 48 hours. ER Ca^{2+} depletion was stimulated with 50 μM ATP in medium with no extracellular Ca^{2+}. n=100 cells per condition. Right: Quantification of Ca^{2+} peak normalized to baseline. n=296 cells for controls and 278 cells for TNFα, averaged from three different biological replicates per condition. ****P<0.0001. (**D**) Left: Immunoblot analysis of protein expression and phosphorylation levels in 3T3-L1 adipocytes treated with or without TNFα (4 ng/ml) for 48 hours. Right: Western blot quantification. n=3 biological replicates per group. *P<0.05. NT, non-treated. (**E**) Left: Immunoblot analysis of protein expression and phosphorylation levels in 3T3-L1 adipocytes treated with or without TNFα (4 ng/ml) for 6, 12, or 24 hours. Right: Western blot quantification. n=3 biological replicates per group. ***P<0.0005 (6 hours); **P<0.01 (12 hours); *P<0.05 (24 hours). (**F**) Left: Immunoblot analysis of protein expression and phosphorylation levels in 3T3-L1 adipocytes treated with or without TNFα (4 ng/ml) for 48 hours. Right: Western blot quantification. n=3 biological replicates per group. Error bars denote SEM. Statistical significance was determined by unpaired t test except (B) and (C) where Mann-Whitney test was used and (E) where one-way ANOVA (followed by Dunnett

test) was used. The experiments in this figure were replicated two times except in (D), which was replicated three times.

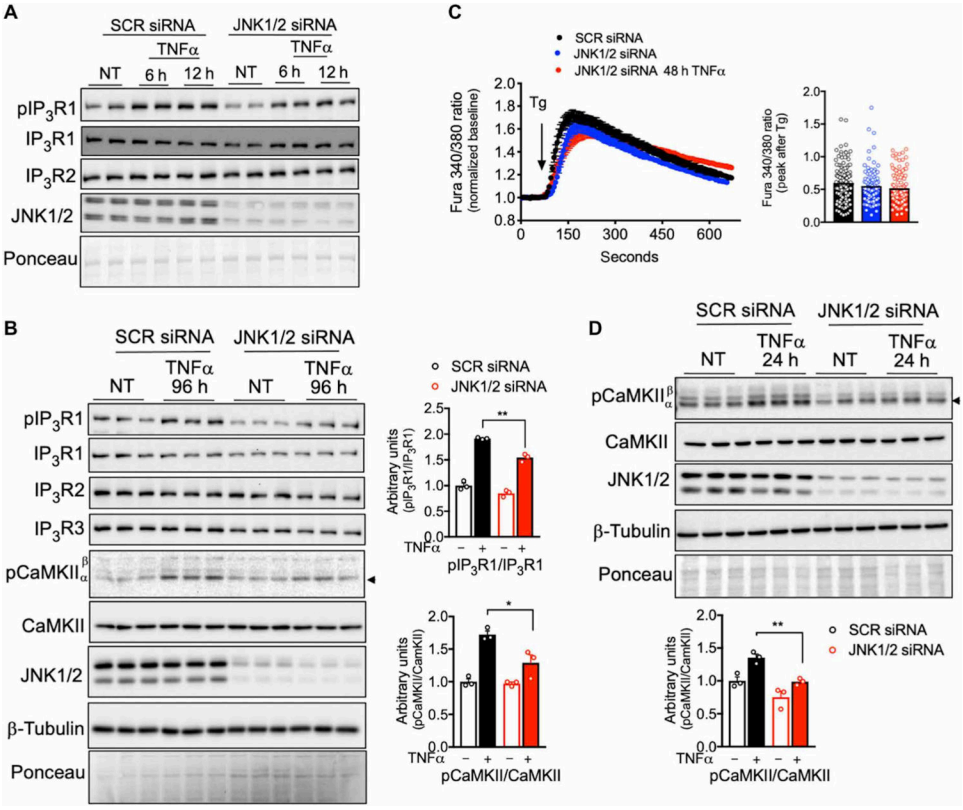

Fig. 2. IP3R1/2 and CaMKII activation by inflammatory stress is dependent on JNK1/2.

(**A**) Left: Immunoblot analysis of protein expression and phosphorylation levels in 3T3-L1 adipocytes transfected with scrambled (SCR) or JNK1/2 siRNA and treated with or without TNFα (4 ng/ml) for 6 and 12 hours. NT, non-treated. (**B**) Left: Immunoblot analysis of protein expression and phosphorylation levels in 3T3-L1 adipocytes transfected with SCR and JNK1/2 siRNA and treated with or without TNFα (4 ng/ml) for 96 hours. Right: Western blot quantification. n=3 biological replicates per group. *P<0.05; **P<0.005. (**C**) Left: Representative Fura-2 AM–based cytosolic Ca^{2+} measurements in differentiated 3T3-L1 adipocytes pretreated with TNFα (4 ng/ml) for 48 hours. Depletion of ER Ca^{2+} was induced with 1 μM thapsigargin in medium with no extracellular Ca^{2+}. n=38 cells for SCR siRNA, 40 cells for JNK1/2 siRNA, and 25 cells for JNK1/2 siRNA + TNFα. Right: Quantification of Ca^{2+} peak normalized to baseline. n=116 SCR siRNA, 106 JNK1/2 siRNA, and 125 JNK1/2 siRNA + TNFα cells, averaged from four different biological replicates. (**D**) Top: Immunoblot analysis of protein and phosphorylation levels in 3T3-L1 adipocytes treated with or without TNFα (4 ng/ml) for 24 hours. Bottom: Western blot quantification. n=3 biological replicates per group. **P<0.005. Error bars denote SEM. Statistical significance was determined by unpaired t test. The experiments in this figure were replicated two times.

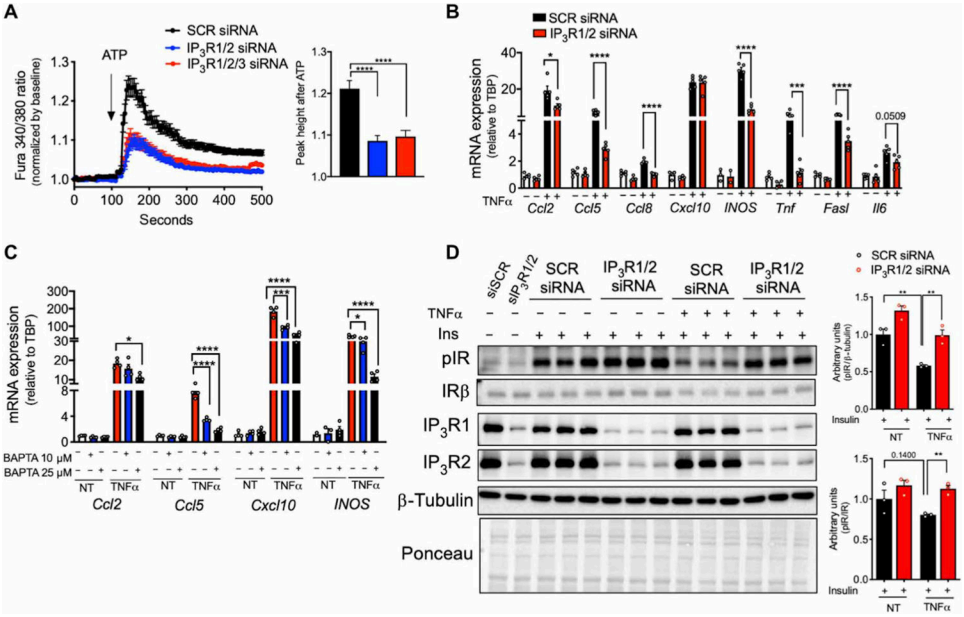

Fig. 3. IP3R suppression or chelation of cytosolic Ca^{2+} in adipocytes impairs TNFα inflammatory and metabolic action.

(**A**) Left: Representative Fura-2 AM–based cytosolic Ca^{2+} measurements in differentiated 3T3-L1 adipocytes transfected with scrambled (SCR), IP3R1/2, or IP3R1/2/3 siRNA. Ca^{2+} release was induced with 50 μM ATP in medium with no extracellular Ca^{2+}. Right: Quantification of the cytosolic Ca^{2+} peak normalized to baseline. n=236 cells for SCR siRNA and 226 cells for IP3R1/2 and IP3R1/2/3 siRNA. ****P<0.0001. (**B**) qPCR analysis of the mRNA levels of the indicated genes in 3T3-L1 adipocytes transfected with SCR and IP3R1/2 siRNA and treated with or without TNFα (4 ng/ml) for 6 hours. n=5 biological replicates per group. *P<0.05 (Ccl2); ****P<0.0001 (Ccl5, Ccl8, INOS, and Fasl); ***P<0.005 (Tnf). (**C**) qPCR analysis of the mRNA levels of the indicated genes in 3T3-L1 adipocytes treated with 10 or 25 μM BAPTA-AM and stimulated with or without TNFα (4 ng/ml) for 6 hours. n=4 biological replicates per group. *P<0.05 (Ccl2), ****P<0.0001 (Ccl5); ***P<0.005; ****P<0.0001(Cxcl10); *P<0.05; ****P<0.0001 (INOS). (**D**) Immunoblot analysis and quantification of insulin signaling in 3T3-L1 adipocytes transfected with SCR or IP3R1/2 siRNA, treated with or without TNFα (4 ng/ml) for 96 hours and with 10 nM insulin for 3 min. n=3 biological replicates per group. **P<0.005. Error bars denote SEM. Statistics were determined by unpaired t test except (A) where Mann-Whitney test was used and (C) where one-way ANOVA (followed by Dunnett test) was used. The experiments in this figure were replicated two times.

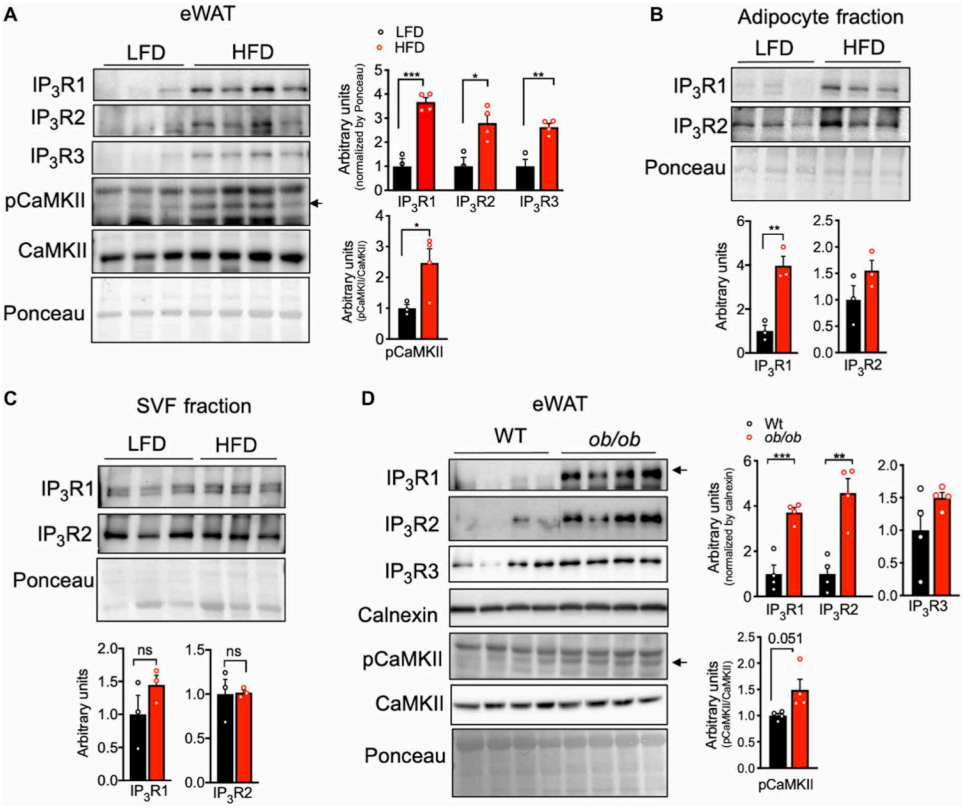

Fig. 4. Obesity leads to increased IP3R expression and CaMKII phosphorylation in adipose tissue.

(**A**) Left: Immunoblot analysis of protein expression and phosphorylation levels in epididymal WAT (eWAT) from mice fed a low-fat diet (LFD) or a high-fat diet (HFD) for 16 weeks. Right: Western blot quantification. n=3 mice LFD and 4 mice HFD. *P<0.05; **P<0.005; ***P<0.001. (**B** and **C**) Left: Immunoblot analysis of protein expression in adipocyte fraction and stromal vascular fraction (SVF) derived from eWAT from mice fed LFD or HFD for 16 weeks. n=3 mice per group. Right: Western blot quantification. n=3 mice per group. *P<0.05. ns, not significant. (**D**) Left: Immunoblot analysis of protein expression and phosphorylation levels in eWAT from WT and leptin-deficient (ob/ob) mice. Right: Western blot quantification. n=4 mice per group. **P<0.005; ***P<0.0005. The experiments in this figure were replicated in two independent mice cohorts.

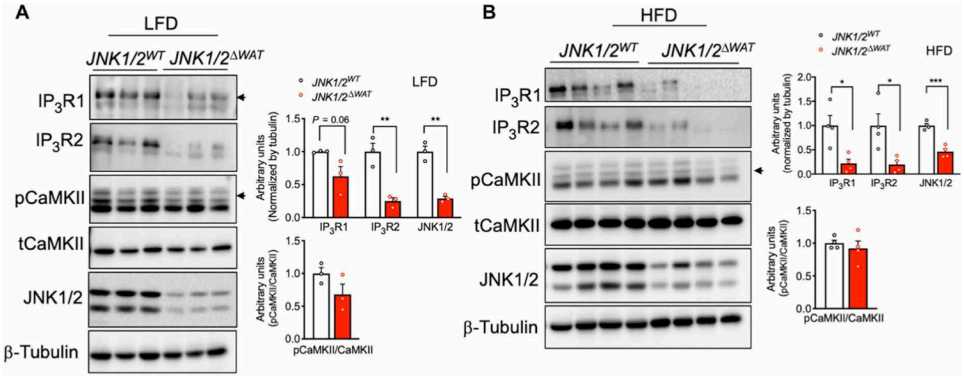

Fig. 5. JNK1/2 deficiency in WAT leads to decreased IP3R abundance.

(**A**) Left: Immunoblot analysis of protein expression and phosphorylation levels in eWAT derived from control mice ($JNK1/2^{WT}$) and mice with an adipocyte-specific loss of JNK1/2 ($JNK1/2^{\Delta WAT}$) fed an LFD. Right: Western blot quantification. n=3 mice per group. (**B**) Left: Immunoblot analysis of protein expression and phosphorylation levels in eWAT derived from control mice ($JNK1/2^{WT}$) and mice adipocyte-specific loss of JNK1/2 ($JNK1/2^{\Delta WAT}$) fed an HFD. Right: Western blot quantification. n=4 mice per group. **P<0.005; *P<0.05; ***P<0.0005. Error bars denote SEM. Statistical significance was determined by unpaired t test. Experiments in this figure were replicated two times in independent mice cohorts.

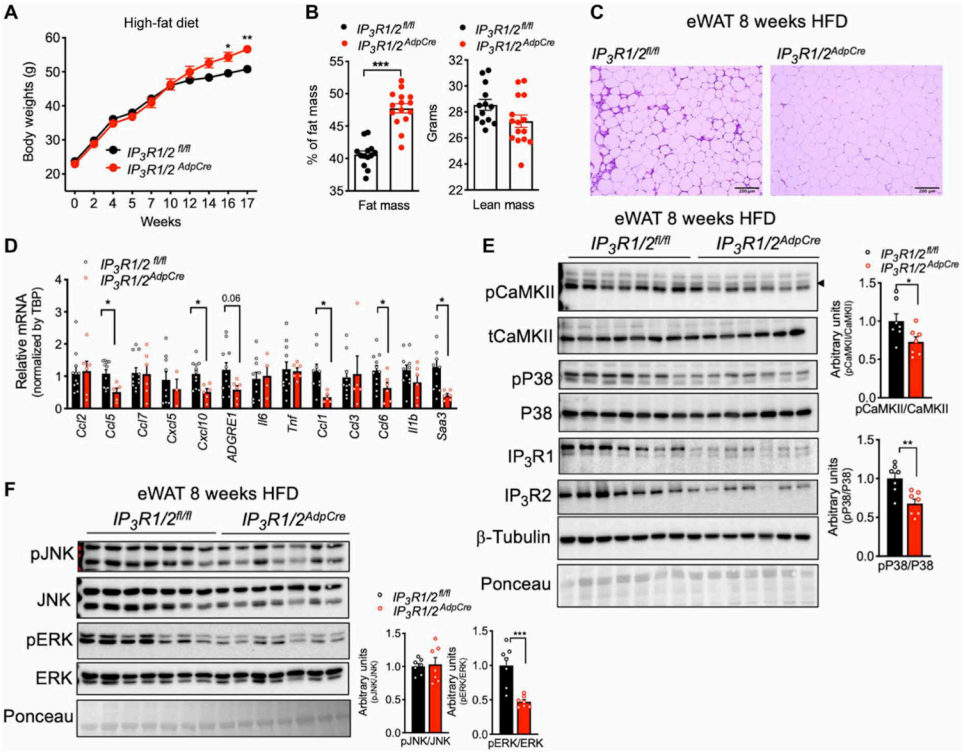

Fig. 6. IP3R1/2 deficiency leads to increased weight gain and decreased adipose tissue inflammation.

(**A**) Weight gain curves of IP3R1/2$^{fl/fl}$ and IP3R1/2^{AdpCre} mice fed an HFD. n=13 IP3R1/2$^{fl/fl}$ mice and 15 IP3R1/2^{AdpCre} mice. *P<0.05; **P<0.005. (**B**) DEXA analysis of whole-body fat and lean mass. n=13 IP3R1/2$^{fl/fl}$ mice and 15 IP3R1/2^{AdpCre} mice. ***P<0.0001. (**C**) Representative hematoxylin and eosin–stained histology sections of eWAT from weight-matched IP3R1/2$^{fl/fl}$ and IP3R1/2^{AdpCre} mice fed an HFD for 8 to 9 weeks. n=10 IP3R1/2$^{fl/fl}$ mice and 6 IP3R1/2^{AdpCre} mice. (**D**) qPCR analysis of the mRNA levels of the indicated genes in eWAT from IP3R1/2$^{fl/fl}$ and IP3R1/2^{AdpCre} mice fed an HFD for 8 to 9 weeks; n=11 IP3R1/2$^{fl/fl}$ mice and 6 IP3R1/2^{AdpCre} mice. *P<0.05 (Ccl5, Cxcl10, Ccl1, Ccl6, and Saa3). (**E**) Left: Immunoblot analysis of protein expression and phosphorylation levels in eWAT lysates from IP3R1/2$^{fl/fl}$ and IP3R1/2^{AdpCre} mice fed an HFD for 8 to 9 weeks. Right: Western blot quantification. n=7 mice per group. *P<0.05; **P<0.005. (**F**) Left: Immunoblot analysis of protein expression and phosphorylation levels in eWAT lysates from IP3R1/2$^{fl/fl}$ and IP3R1/2^{AdpCre} mice fed an HFD for 8 to 9 weeks. Right: Western blot quantification. n=7 mice per group. ***P<0.005. Error bars denote SEM. Statistical significance was determined by unpaired t test except (A) where a two-way ANOVA (followed by Sidak's test) was used. The experiment in (A) was replicated in three independent mice cohorts.

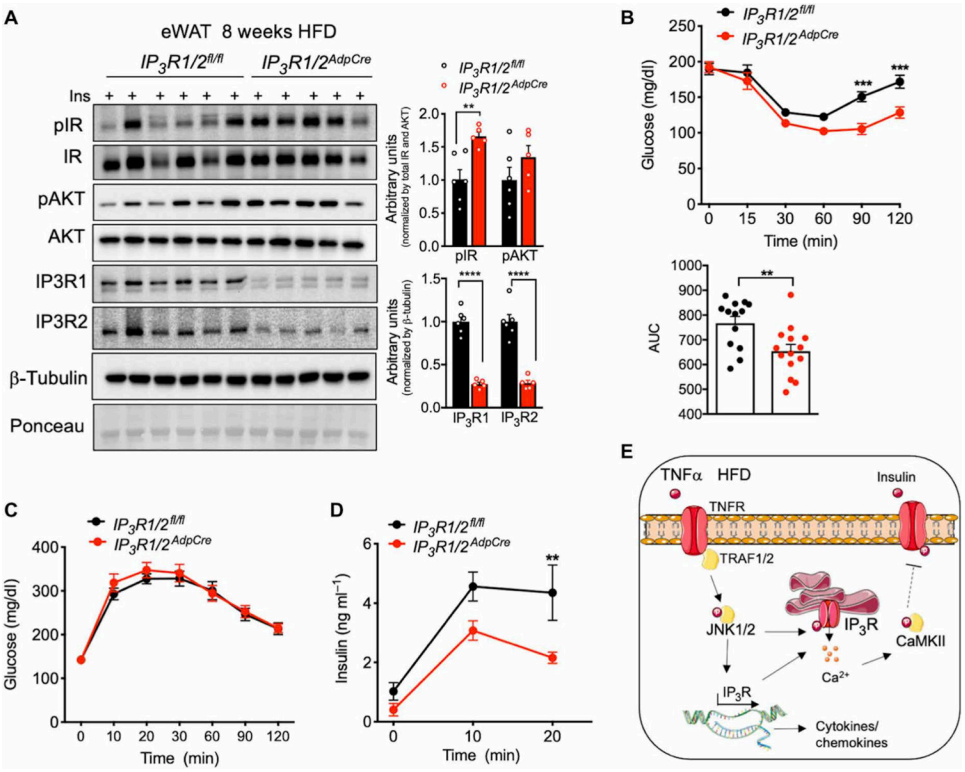

Fig. 7. IP3R1/2 deficiency leads to increased insulin sensitivity.

(**A**) Left: Markers of insulin signaling evaluated by immunoblot analysis of total eWAT from mice injected with insulin (0.45 U/kg). Tissues were collected 3 min after injection. Right: Quantification of the phosphorylation of the indicated proteins normalized to total protein levels. n=6 IP3R1/2$^{fl/fl}$ mice and 5 IP3R1/2^{AdpCre} mice. **P<0.005; ****P<0.0001. (**B**) Top: Insulin tolerance test in IP3R1/2$^{fl/fl}$ and IP3R1/2^{AdpCre} mice fed an HFD for 16 weeks. ***P<0.001. Bottom: Quantification of the area under the curve (AUC). n=13 IP3R1/2$^{fl/fl}$ mice and 14 IP3R1/2^{AdpCre} mice. **P<0.01. (**C**) Oral glucose tolerance test in IP3R1/2$^{fl/fl}$ and IP3R1/2^{AdpCre} mice fed an HFD for 10 weeks. n=13 IP3R1/2$^{fl/fl}$ mice and 15 IP3R1/2^{AdpCre} mice. (**D**) Insulin levels during the oral glucose tolerance test. **P<0.005 (20 min). (**E**) Working model. Error bars denote SEM. Statistical significance was determined by unpaired t test except (B) and (D) where two-way ANOVA (followed by Sidak's test) was used. Experiments presented in (B) to (D) were replicated in two independent mice cohorts.